Isomers and energy landscapes of micro-hydrated sulfite and chlorate clusters

Hey, John; Doyle, Emily; Chen, Yuting; Johnston, Roy L.

Link to publication on Research at Birmingham portal

Research

Author for correspondence:
Roy L. Johnston
e-mail: r.l.johnston@bham.ac.uk

THE ROYAL SOCIETY
PUBLISHING

Isomers and energy landscapes of micro-hydrated sulfite and chlorate clusters

John C. Hey, Emily J. Doyle, Yuting Chen and Roy L. Johnston

School of Chemistry, University of Birmingham, Birmingham B15 2TT, UK

JCH, 0000-0002-2828-1006

We present putative global minima for the micro-hydrated sulfite $SO_3^{2-}(H_2O)_N$ and chlorate $ClO_3^-(H_2O)_N$ systems in the range $3 \leq N \leq 15$ found using basin-hopping global structure optimization with an empirical potential. We present a structural analysis of the hydration of a large number of minimized structures for hydrated sulfite and chlorate clusters in the range $3 \leq N \leq 50$. We show that sulfite is a significantly stronger net acceptor of hydrogen bonding within water clusters than chlorate, completely suppressing the appearance of hydroxyl groups pointing out from the cluster surface (dangling OH bonds), in low-energy clusters. We also present a qualitative analysis of a highly explored energy landscape in the region of the global minimum of the eight water hydrated sulfite and chlorate systems.

This article is part of the theme issue 'Modern theoretical chemistry'.

1. Introduction

Ions can be classified according to the Hofmeister series, which orders ions according to their ability to de-solvate proteins [1–5]. The ions which promote disorder within the hydrogen-bonding network of water and disrupt protein stability are labelled as chaotropes, while ions which promote long-range order and protein stability within water are classified as kosmotropes [1, 2, 6]. The hydration of ions is also important as it has a large bearing on the atmospheric nucleation of

water clusters and other areas of atmospheric science [7–9]. We have previously studied the chaotropic perchlorate (ClO_4^-) and the kosmotropic sulfate (SO_4^{2-}) ions in finite gas-phase water clusters [10–12].

The SO_2 released from natural and synthetic sources is quickly oxidized in the atmosphere to form sulfur(IV) and sulfur(VI) species. Sulfite (SO_3^{2-}) and other sulfur(IV) ions are commonly found in inorganic aerosols, which are important in atmospheric science as they contribute to the formation of acid rain [8,13–15]. There have been several studies focusing on sulfite in the past [8, 16,17] and sulfite has been shown to be kosmotropic in molecular dynamics simulations with model proteins [17]. Chlorate (ClO_3^-) is isoelectronic with sulfite and shares a similar geometry, with a lower charge and thus provides a useful comparison with sulfite.

2. Methods

An empirical potential has been chosen to allow for fast and efficient searching of a large range of cluster sizes. The interaction energy (U) is evaluated as the sum of Coulombic and Lennard–Jones contributions over all pairs of interacting sites (atoms and pseudoatoms);

$$U = \sum_{i=1}^{N} \sum_{j=i+1}^{N} \left\{ \frac{q_i q_j}{r_{ij}} + 4\epsilon_{ij} \left[\left(\frac{\sigma_{ij}}{r_{ij}} \right)^{12} - \left(\frac{\sigma_{ij}}{r_{ij}} \right)^{6} \right] \right\}, \tag{2.1}$$

where r_{ij} is the inter-site separation, σ_{ij} and ϵ_{ij} are the Lennard–Jones energy and distance parameters, and q_i and q_j are the charges on sites i and j, respectively.

The Lennard–Jones parameters used for sulfite were derived using Moller–Plesset MP4(SDTQ) *ab initio* calculations [18]. The sulfite ion is modelled as a rigid pyramidal species with O–S–O bond angles of 106° and S–O bond lengths of 1.9 Å. The sulfur atom is 0.76 Å out of the plane of the three oxygen atoms. The Lennard–Jones parameters and partial charges used for chlorate were taken from the literature and were determined by *ab initio* LCAO MO SCF calculations [19,20]. The chlorate ion is also modelled as a rigid pyramidal species, the O–Cl–O bond angles are 105.8° and the Cl−O bond lengths are 1.48 Å. The chlorine atom is 0.58 Å out of the plane of the oxygen atoms. The partial charges for both ions were calculated in this work using the Bader method [21] within the NWChem [22] DFT package using the B3LYP exchange correlation functional and the 6-311++G** basis set, the charges were calculated for a lone ion in the gas phase.

Water molecules in this study are modelled using the TIP4P potential: a rigid four-site molecule is defined with a H−O−H bond angle of 104.52°, with an oxygen lone-pair site represented by a pseudoatom which carries the charge of the oxygen atom but has no Lennard–Jones parameters. The TIP4P potential has been shown to replicate many of the properties of bulk water, while also being computationally inexpensive to model [23–25]. The Lennard–Jones and partial charges are listed in table 1.

Low-energy minima on the potential energy surface for the ion-water clusters were explored using the basin-hopping Monte Carlo algorithm developed by Wales and co-workers within the pele package [26,27]. Basin-hopping was used to identify a putative lowest energy structure (global minimum, GM), to efficiently search the potential energy landscape and to create a database of low-energy minima for later mapping of the landscape [26,28]. Ten basin-hopping runs of 500 000 steps were performed in parallel for each size of XO_3^{q-} ($H_2O)_N$ cluster in the range $3 \leq N \leq 50$.

The geometry perturbations implemented in this study were performed in blocks of 100 moves of the same type, with minimizations performed after each perturbation. The three move classes implemented are random translations, random rotations and cycle inversion moves. The translation moves apply random translation vectors to molecules within the cluster. Rotation moves apply random rotation vectors in the range $\pm\pi$ radians to all of the molecules within the cluster. The cycle inversion moves were performed using the method outlined in our previous work [10–12], first proposed by Takeuchi [29].

Table 1. Table of Lennard–Jones parameters and partial charges used for sulfite, chlorate and TIP4P water in this study [18].

site	ϵ (kcal mol^{-1})	σ (Å)	$q(e)$
$S_{SO_3^{2-}}$	0.25	3.6	0.281
$O_{SO_3^{2-}}$	0.25	3.2	−0.760
$Cl_{ClO_3^-}$	0.040	4.86	0.452
$O_{ClO_3^-}$	0.076	3.10	−0.484
O_{H_2O}	0.648	3.2	0
H_{H_2O}	0	0	0.52
LP_{H_2O}	0	0	−1.04

For the landscape exploration of the hydrated sulfite and chlorate systems, the doubly nudged elastic band method [28] was used to search for transition states between minima found during global optimization. Pathways are found by sampling between end points using a linear interpolation of the translational coordinates of the rigid-body molecules and spherical linear quaternion interpolation of the rotational coordinates [30]. Candidate transition states are then further optimized using hybrid eigenvector following [31,32]. The resultant energy landscapes are visualized as disconnectivity graphs using the PyConnect package [33].

3. Results

(a) Global optimization

The putative GM structures for $SO_3^{2-}(H_2O)_N$ clusters in the range $1 \leq N \leq 16$, which are shown in figure 1, display a preference for high-symmetry structures at small sizes.

For structures with $N \geq 19$, the water molecules complete the first solvation shell around the sulfite ion, which adopts a central position in the cluster. There is a void within the cluster inside a cage-like water structure above the sulfur atom of the sulfite for structures with $N \geq 19$, although there is some coulombic attraction between the positively charged S atom and the negative pseudoatom of the TIP4P water molecules, which carries the partial charge of the oxygen site. The small sulfite clusters ($N \leq 12$) show a high preference for the formation of trimeric hydrogen bond rings, with all of the clusters in this range exhibiting trimeric rings as the only closed loops in their hydrogen-bonding networks, which is similar to the behaviour observed for sulfate ions in previous work [11]. The putative global minima for the chlorate system are presented in figure 2. The hydrated chlorate clusters generally have structural motifs similar to those seen in finite water clusters, displaying a preference for stacked cubes, pentagons and hexagons, which are commonly seen in water clusters [34]. The chlorate ion displays a marked preference for occupying surface sites in the clusters, occupying these sites for all sizes of cluster studied. This preference for water-like structural motifs leads to the chlorate clusters generally having lower symmetry than the corresponding sulfite clusters. As the size of the clusters increases, both systems exhibit larger hydrogen-bonding rings, which are common in large pure-water clusters. At these larger sizes, the sulfite continues to occupy sub-surface sites, and the chlorate continues to occupy surface sites.

From figure 3, it can be seen that in the range $1 \leq N \leq 15$, the same lowest energy structure is found by the majority of the independent basin-hopping runs for both ionic systems. For larger sizes, the number of independent runs converging on the same minimum falls rapidly, reflecting the rapid rise in the number of minima with cluster size. The confidence in having identified the true GM for both systems decreases, but we still believe that we find a representative sample of low-energy minima on which analysis can be performed.

4

rsta.royalsocietypublishing.org   Phil. Trans. R. Soc. A **376**: 2017.0154
....
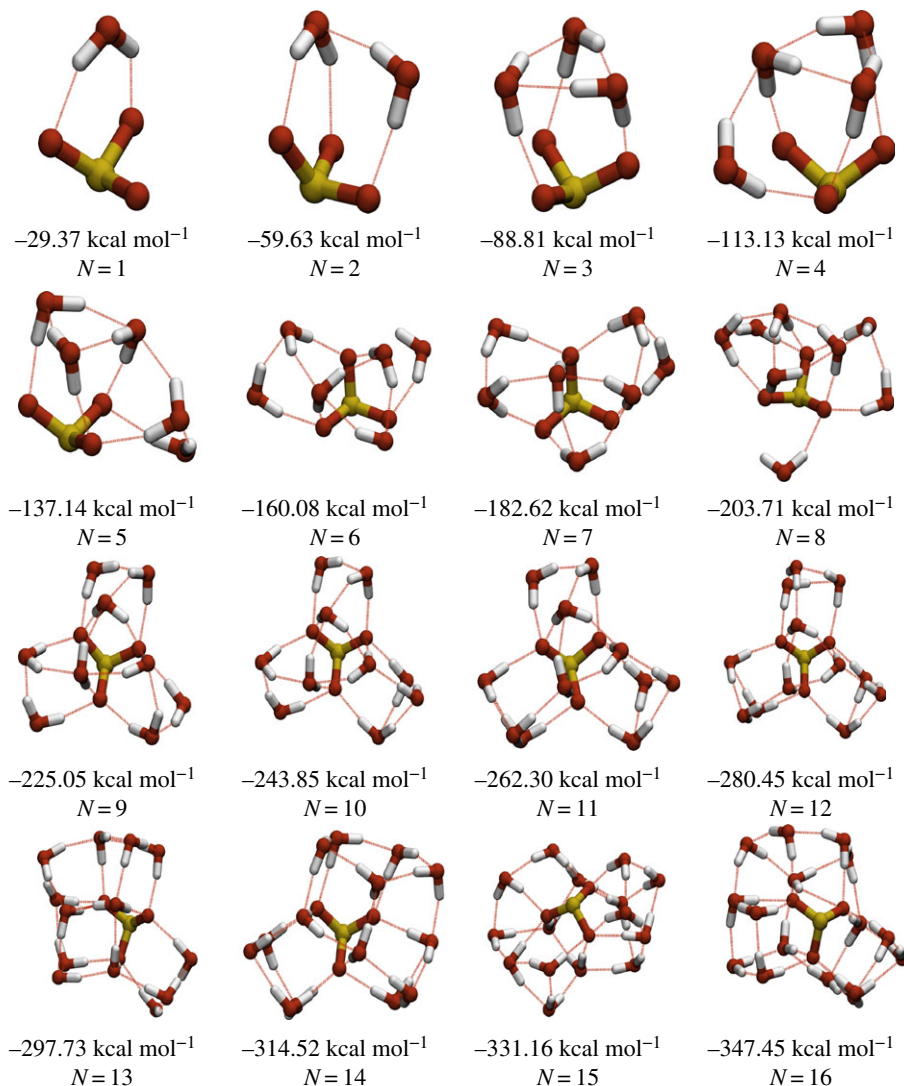
Figure 1. Table of lowest energy minima for the $SO_3^{2-}(H_2O)_N$ system in the range $3 \leq N \leq 16$. Electronic supplementary material, ESM2, contains the coordinates and energies for the putative global minima in the range $3 \leq N \leq 50$. (Online version in colour.)

For verification of our potential, we locally re-optimize a number of low-energy minima at the density functional theory (DFT) level, using the B3LYP exchange correlation functional and the 6-311++G** basis set and D3 dispersion corrections, as implemented within the NWChem package [22].

Figure 4 shows the correlation between the DFT and empirical energies for the 10 lowest energy $SO_3^{2-}(H_2O)_3$ and $ClO_3^-(H_2O)_3$ minima when re-optimized at the DFT level. The lowest energy minimum found at the empirical level remains the lowest in energy at the DFT level for both the chlorate and sulfite systems. Some of the initial minima are almost degenerate in energy, and thus there is some overlap. Several of the non-degenerate sulfite minima re-optimize to the same minimum on the DFT landscape. This simplification of the DFT landscape when compared with the empirical landscape has been noted in some of our previous work [10]. The re-optimized minima all share the same oxygen framework as their parent empirical minima, with some lengthening seen in the water–water hydrogen bonds. This would likely be improved by
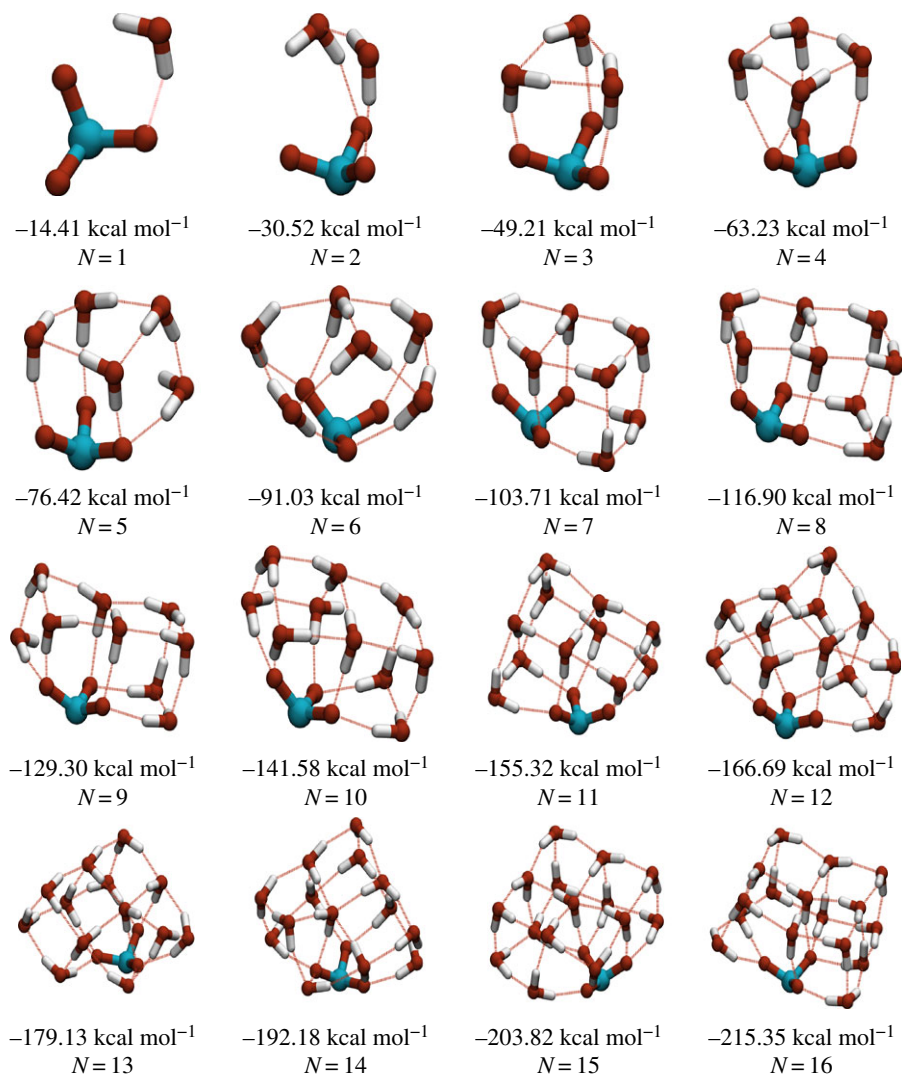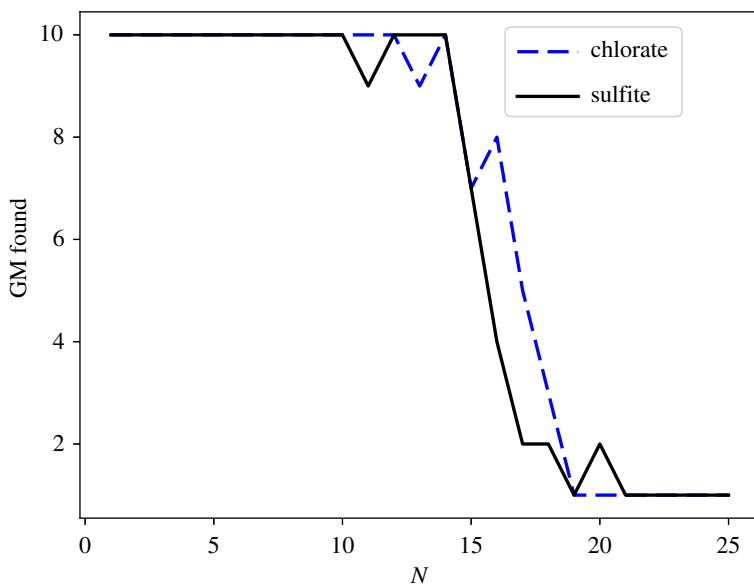
Figure 2. Table of lowest energy minima for the $ClO_3^-(H_2O)_N$ system in the range $3 \leq N \leq 16$. Electronic supplementary material, ESM1, contains the coordinates and energies for the putative global minima in the range $3 \leq N \leq 50$. (Online version in colour.)

the use of a polarizable empirical water model. When re-optimizing small numbers of minima for larger sizes (up to $N = 12$), there is generally a good agreement between the energetic ordering of the empirical and DFT minima, although this does worsen as expected for larger sizes. The agreement is perhaps not surprising, as the empirical potentials for chlorate and sulfite are fitted to high level methods [18–20] and the charges used for the ions are calculated using the same DFT functional and basis set as used in our re-optimizations [22]. This is consistent with the observations made in our previous work [10–12].

The evolution of interaction energy per water molecule in the range $1 \leq N \leq 50$, shown in figure 5, is obtained by Boltzmann weighting according to equation (3.1):

$$\frac{\bar{U}}{N} = \frac{\sum_i e^{-\Delta U \beta} \frac{U}{N}}{\sum_i e^{-\Delta U \beta}}, \tag{3.1}$$

6

rsta.royalsocietypublishing.org *Phil. Trans. R. Soc. A* **376**: 20170154


Figure 3. Number of parallel basin-hopping runs which converge on the same lowest energy minimum (GM) structure for hydrated chlorate and sulfite ions with 1–25 water molecules. (Online version in colour.)
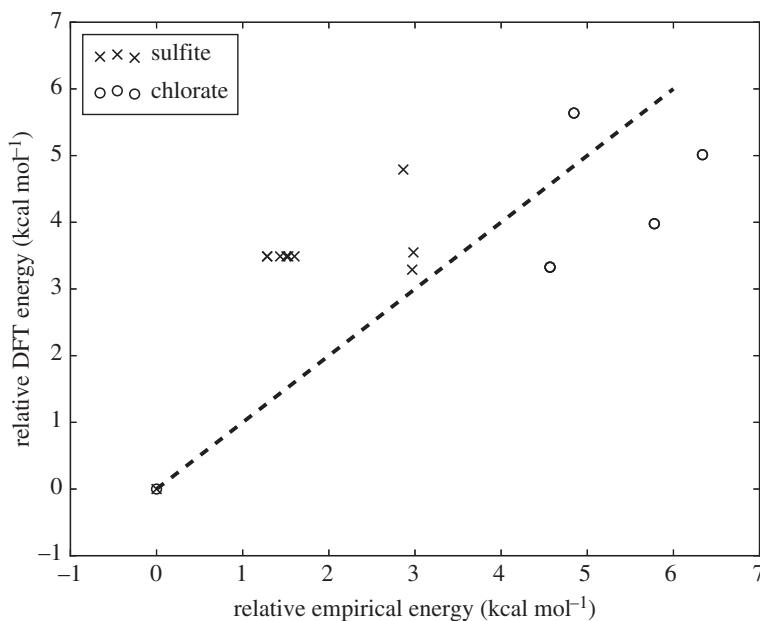
Figure 4. Locally minimized DFT versus empirical energies for the 10 lowest energy minima found for $N = 3$ on the empirical landscapes of the sulfite and chlorate systems. Energies are given relative to the respective global minima. The dashed line corresponds to the location of perfectly correlated minima.

where ΔU is the interaction energy of cluster i above the putative GM, $\beta = 1/k_{B}T$ and the average interaction energy per water molecule is denoted by $\bar{U}/N$. The weighted mean is taken over all structural isomers of unique energy found in all basin-hopping runs for each size of cluster. A theoretical temperature of $130\,\mathrm{K}$ is used to maintain consistency with previous computational
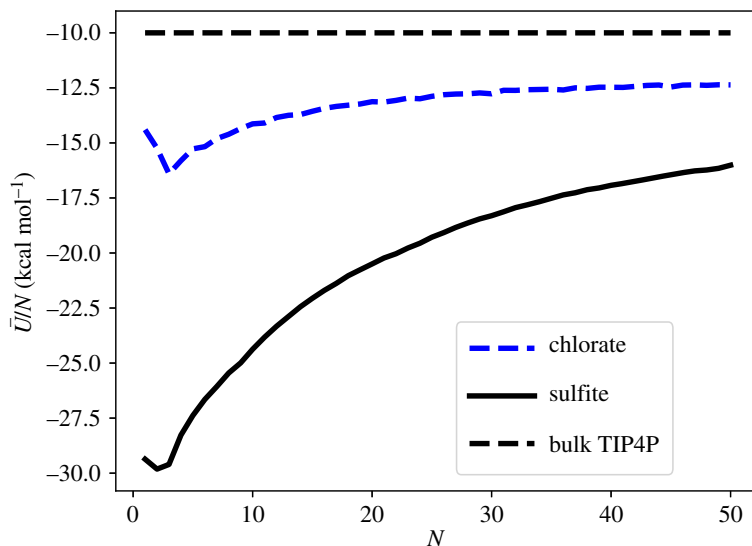
Figure 5. Boltzmann weighted interaction energy per water molecule for $SO_3^{2-}(H_2O)_N$ and $ClO_3^-(H_2O)_N$ clusters in the range $1 \le N \le 50$. (Online version in colour.)

work [10,11] based on the experimental studies of the hydrated sulfate ion [14]. Figure 5 shows that the asymptotic limit for the interaction energy for TIP4P water in the bulk ($\approx -10\,\text{kcal mol}^{-1}$) has not yet been reached at $N = 50$. The decreasing magnitude of $\bar{U}/N$ with increasing N is due to the dilution effect of the single ion. The deviation from the TIP4P asymptote is greatest for sulfite–water clusters, due to the higher charge of the sulfite ion, leading to a larger coulombic interaction between the TIP4P water molecules and the ion.

It was shown experimentally by Williams and co-workers [14] and computationally by Smeeton *et al.* [11] that the sulfate ion (SO_4^{2-}) promotes long-range order within water nano-droplets, with total suppression of hydroxyl groups protruding from the surface of the cluster, (dangling O−H bonds), for all sizes in the range $18 \le N \le 43$.

(b) Structural characterization

Figure 6 shows that the sulfite ion also promotes long-range order within the water clusters by totally suppressing the appearance of dangling O−H bonds for every optimized cluster found with $\Delta U \le 5\,\text{kcal mol}^{-1}$ in the range $1 \le N \le 50$. The presence of the sulfite ion induces all the hydrogen atoms of the water molecules in the clusters to interact either with the oxygen atoms of the other water molecules or directly with the oxygen atoms of the sulfite ion. Owing to the higher negative charge localized on the oxygen atoms of the sulfite ion (since the negative charge is spread only over three oxygen atoms), this effect is stronger for sulfite than sulfate, with the effect dominating well into the formation of the third solvation shell. This effect is seen, to a lesser degree, in the chlorate system, with the chlorate ion providing a greater degree of patterning than the perchlorate system [10]. There is complete suppression of the appearance of dangling O−H bonds in chlorate–water clusters with $3 \le N \le 18$. In the larger clusters, there are fewer unbonded hydroxyl groups than are reported for the equivalent perchlorate clusters, for all sizes.
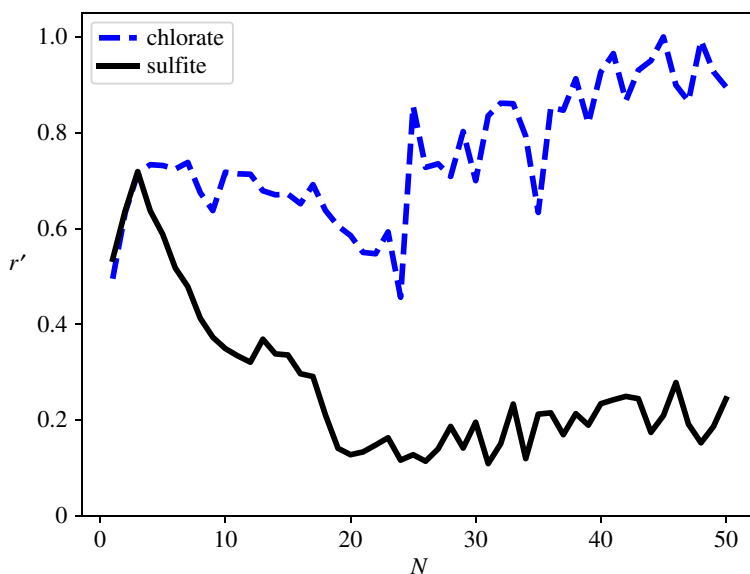
The ratio of the displacement, (r), of the centre of mass of each ion to the radius of gyration, (r_{gyr}), of the cluster for the 1000 lowest energy clusters is Boltzmann weighted according to the following equation:

$$r' = \frac{\sum_i e^{-\Delta U \beta}(r/r_{\text{gyr}})}{\sum_i e^{-\Delta U \beta}}, \tag{3.2}$$
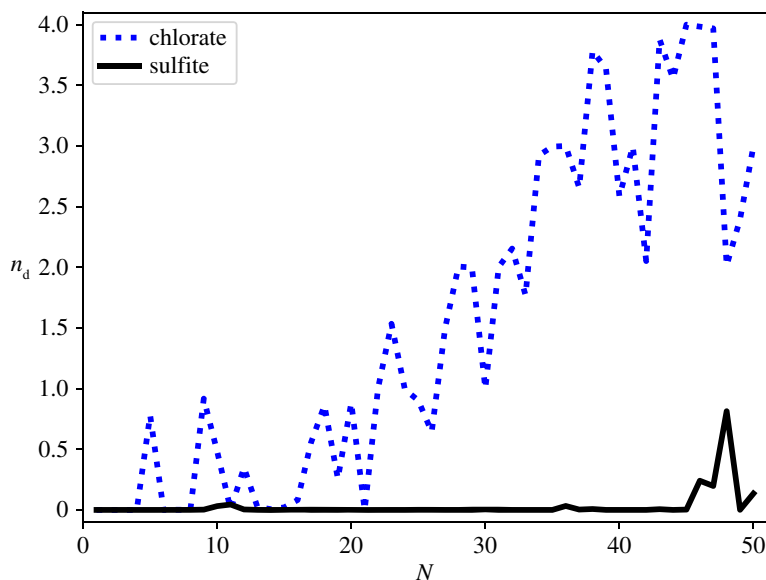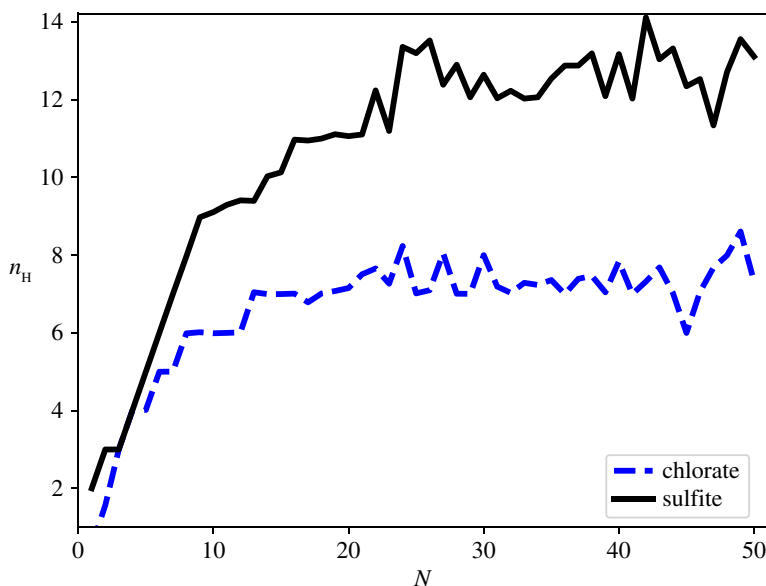
Figure 6. Boltzmann weighted mean number of dangling hydrogen bonds (n_d) for SO_3^{2-} (H_2O)$_N$ and ClO_3^- (H_2O)$_N$ clusters in the range $1 \leq N \leq 50$. (Online version in colour.)

Figure 7. Displacement r' of the chlorate and sulfite ions within the cluster in the range $1 \leq N \leq 50$. (Online version in colour.)

where ΔU is the energy of minimum i above the GM, r is the displacement of the centre of mass of the sulfite ion from the centre of mass of the water molecules in cluster i, and $\beta = 1/k_B T$. Figure 7 shows that for clusters in the range $1 \leq N \leq 8$ the sulfite ion lies on the surface of the cluster, i.e. the formation of the water cage around the sulfur site has not yet begun. For clusters with $12 \leq N \leq 19$, there is a decreasing displacement of the ion from the centre of the cluster as the cage forms around the sulfur atom, and thus the first solvation shell is completed. The displacement then remains relatively constant until $N = 29$, due to the spherical growth of the second hydration

Figure 8. Boltzmann weighted mean number of hydrogen bonds n_H coordinated to the ion in the range $1 \leq N \leq 50$. (Online version in colour.)

shell. At larger sizes, as the third solvation shell forms, we see the emergence of features very common to pure water clusters, namely stacked cubes, pentamers and hexamers, although we do not see the emergence of the dangling hydrogen bonds which are normally prevalent in those structural features in pure water clusters. The sulfite does not remain at the centre of the cluster, but instead favours subsurface sites.

The Boltzmann weighted mean total number of hydrogen bonds donated by the water molecules of the cluster to the ion is shown in figure 8. The Boltzmann weighting is performed across the 1000 lowest energy minima identified by the global optimization. The sulfite ion consistently accepts a greater number of hydrogen bonds than the chlorate ion. This is consistent with the preference of the more highly charged sulfite ion for subsurface sites in contrast with the chlorate which favours surface sites, with the sulfite ion being more accessible to donating water molecules than the chlorate ion at each size. The sulfite ion is observed to coordinate to up to around 14 water molecules with four/five hydrogen bonds donated to each oxygen atom in the ion. The chlorate ion, in contrast, coordinates to a maximum of nine water molecules, with a maximum of three hydrogen bonds donated to each oxygen atom.

(c) Energy landscapes

The energy landscapes of the $SO_3^{2-}(H_2O)_8$ and $ClO_3^-(H_2O)_8$ systems were extensively searched using the method outlined above. The potential energy landscape seen for these cluster sizes is typical of the landscapes searched for the small clusters, and is presented here because they are the most extensively searched.

It can be seen from figure 9 that there is a strong directing effect across the wider sulfite landscape towards the basin containing the proposed GM. The landscape is, therefore, highly funnelled, with relatively low barriers separating local minima from the GM basin. This, coupled with the relatively low number of minima and the efficiency of the basin-hopping search algorithm, explains why sulfite-water clusters in the size range $3 \leq N \leq 13$ are found in all 10 basin-hopping runs. Figure 10 shows the three lowest energy minima found in the landscape of the $SO_3^{2-}(H_2O)_8$ system. There is a barrier of $0.8\,kcal\,mol^{-1}$ separating the GM (Min1) from local

10

rsta.royalsocietypublishing.org   Phil. Trans. R. Soc. A **376**: 20170154
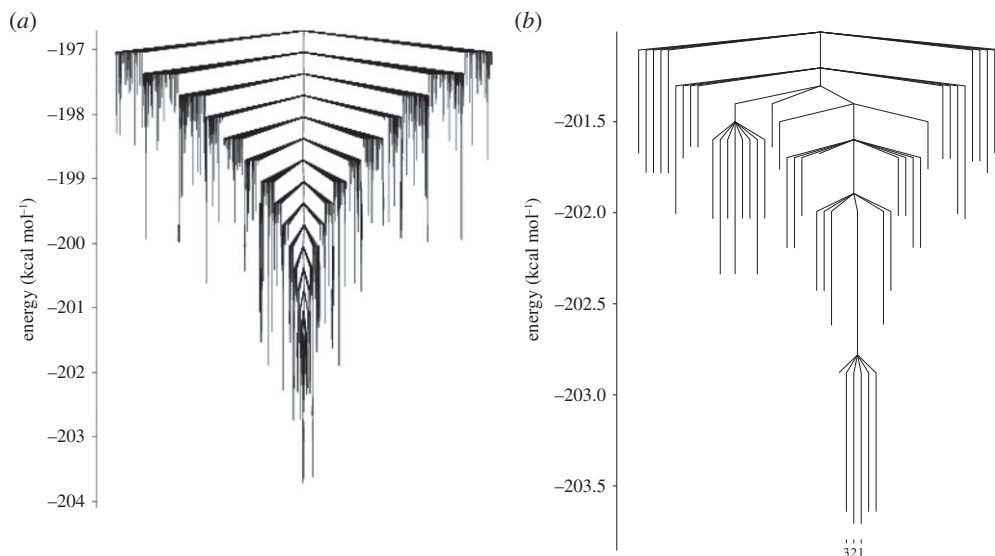
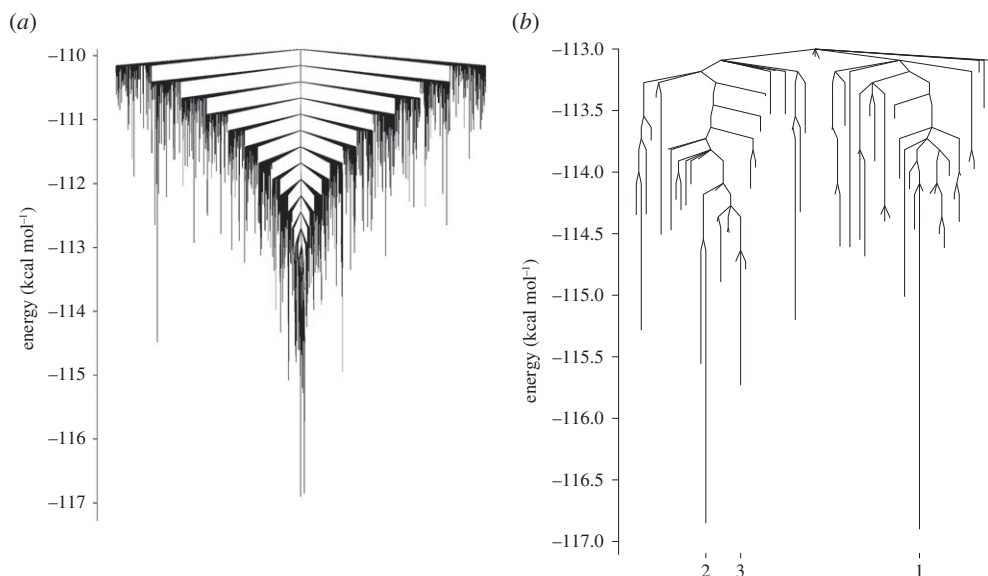**Figure 9.** Disconnectivity graphs showing the putative GM and connected minima for the $SO_3^{2-}(H_2O)_8$ system. The explored landscape comprises 18 860 minima and 425 478 connecting transition states. The graphs show connected minima within (a) 7 and (b) 2.8 kcal mol^{-1} of the GM, with the three lowest energy minima labelled in (b).
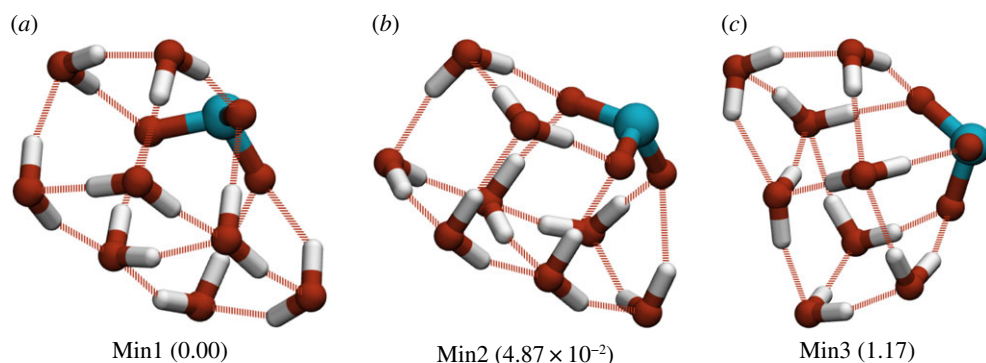

Min1 (0.00)   Min2 (1.66×10^{-4})   Min3 (1.19×10^{-3})
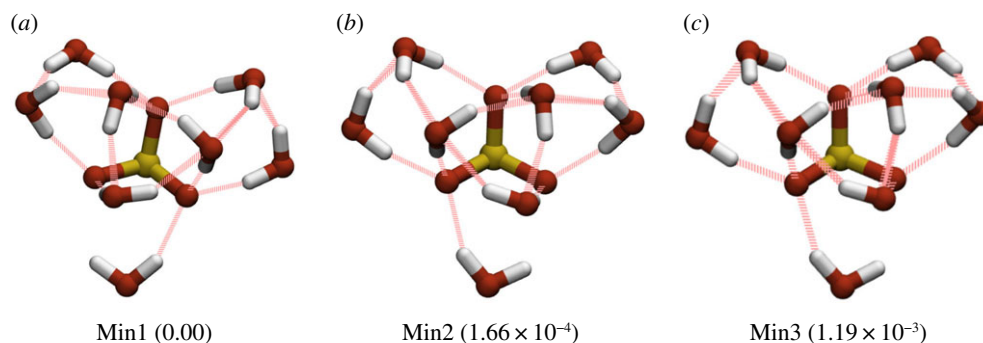
Figure 10. Three lowest energy minima for $SO_3^{2-}(H_2O)_8$. Energies (in kcal mol^{-1}) relative to the GM energy are given in parentheses. (Online version in colour.)

minimum (Min2). These minima are almost degenerate in terms of energy, they have the same oxygen framework, with the only structural difference being a reversal of the direction of the trimeric hydrogen bond ring. The three next lowest minima are slightly higher in energy, and the barrier from the GM is around 0.8 kcal mol^{-1}. One of these minima is pictured in figure 10 (Min3). These minima have similar oxygen frameworks to the GM, but with the trimeric water rings rotated relative to the sulfite oxygens.

The landscape for the $ClO_3^-(H_2O)_8$ system is presented as a disconnectivity graph in figure 11. This landscape is well searched with approximately 36 000 minima and approximately 930 000 connected transition states. There is a pronounced funnelling effect also seen in this landscape, but it is less pronounced than that which is seen in the sulfate system. There is a relatively large barrier of around 3.5 kcal mol^{-1} separating the GM from the next lowest energy minimum. This barrier corresponds to an inversion in the direction of a tetrameric hydrogen bond cycle, this can be seen in figure 12. The GM (Min1) and the next lowest energy minimum (Min2) both share the

Figure 11. Disconnectivity graph showing the putative GM and connected minima for the $ClO_3^{2-}(H_2O)_8$ system. The explored landscape comprises 36 374 minima and 929 171 connecting transition states. Showing connected minima within (a) $\approx 7\,\mathrm{kcal\,mol^{-1}}$ of the GM and (b) $\approx 4\,\mathrm{kcal\,mol^{-1}}$ of the GM, with the three lowest energy minima highlighted.

Min1 (0.00)   Min2 (4.87×10^{-2})   Min3 (1.17)

Figure 12. Three lowest energy minima for $ClO_3^-(H_2O)_8$. Energies (in $\mathrm{kcal\,mol^{-1}}$) relative to the GM energy are given in parentheses. (Online version in colour.)

same oxygen framework, which takes the form of a double-stacked cube similar to the GM found for the pure $TIP4P_{12}$ cluster [34]. In these 8-water chlorate clusters, the oxygens of the chlorate take the place of four of the water molecules in the structure. As the chlorate acts as a net acceptor of hydrogen bonds, this leads to the suppression of the four dangling hydrogen bonds normally seen in the equivalent pure water cluster. The next lowest energy minimum (Min3) adopts a different structure to the other two minima, forming a single cube, with two water molecules capping one face.

The pathway for the transition between Min1 and Min2 has been extracted and the energies of the minima and transition states are presented in figure 13. The first transition state has an energy of $6.5\,\mathrm{kcal\,mol^{-1}}$ above the GM and corresponds to a significant lengthening of one of the hydrogen bonds in the ring as a water molecule moves out of position. This allows the other hydrogen bonds in the ring to relax and form a trimer. The next-transition state corresponds
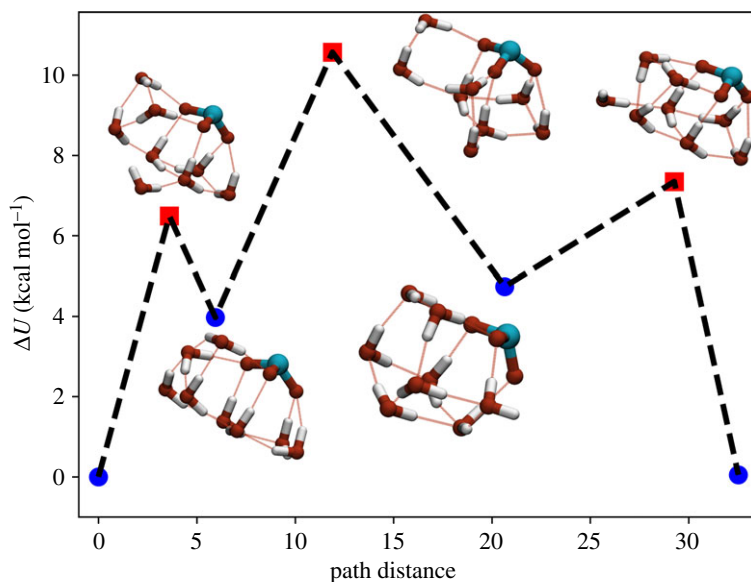
Figure 13. Plot of the pathway between the putative GM (Min1, left) and the second lowest energy minimum (Min2, right) for the ClO_3^- $(H_2O)_8$ system. This pathway consists of an inversion in the direction of the hydrogen bond tetramer. (Online version in colour.)

to another hydrogen bond breaking, to give just two water dimers. This can then relax into a stacked pentamer arrangement with the chlorate oxygens occupying two of the water sites, in a structure similar to the GM of the pure $TIP4P_{10}$ cluster. The next-transition state corresponds to the reformation of a trimeric water ring, before this relaxes to reform the water tetramer.

4. Conclusion

We present putative global minima for the hydrated sulfite and chlorate systems in the range $3 \leq N \leq 16$. Using our simple potential model, the sulfite ion is shown to prefer sub-surface sites to surface sites within the water cluster. We show that the sulfite ion exhibits a greater patterning effect on the hydrogen-bonding networks of clusters than the strong kosmotropic sulfate ion. Conversely, the chlorate ion is shown to favour surface sites on the water cluster, and confers a lesser degree of patterning to the hydrogen-bonding network within the water clusters, the effect is stronger than that previously shown for the perchlorate ion using the same model, but less pronounced than the effect of sulfate.

Extensively searched energy landscapes are presented for the $SO_3^{2-}(H_2O)_8$ and $ClO_3^-(H_2O)_8$ systems and presented alongside some of the low-energy minima from the landscapes. There is shown to be a strong funnelling effect towards the formation of the GM in the potential energy landscapes of small sulfite-water clusters. A less pronounced funnelling effect is seen for the chlorate system. In both cases, the funnelling effect is stronger than the equivalent $XO_4^{q-}(H_2O)_N$ systems.

The obvious future direction of this work is to use a more complex model which accounts for polarization of the ions and water molecules. There are several ways in which we can accomplish this, either by using one of the several polarizable empirical potentials such as iAMOEBA [35,36] or by searching directly at a higher level of theory such as HF or DFT with a small basis set.

13

rsta.royalsocietypublishing.org Phil. Trans. R. Soc. A 376: 20170154

References

1. Cacace MG, Landau EM, Ramsden JJ. 1997 The Hofmeister series: salt and solvent effects on interfacial phenomena. *Q. Rev. Biophys.* **30**, 241–277. (doi:10.1017/S0033583597003363)
2. Xie WJ, Gao YQ. 2013 A simple theory for the hofmeister series. *J. Phys. Chem. Lett.* **4**, 4247–4252. (doi:10.1021/jz402072g)
3. Xie WJ, Gao YQ. 2013 Ion cooperativity and the effect of salts on polypeptide structure— a molecular dynamics study of BBA5 in salt solutions. *Faraday. Discuss.* **160**, 191–206. (doi:10.1039/c2fd20065a)
4. Pokorná J, Heyda J, Konvalinka J. 2013 Ion specific effects of alkali cations on the catalytic activity of HIV-1 protease. *Faraday. Discuss.* **160**, 359–370. (doi:10.1039/c2fd20094e)
5. Light TP, Corbett KM, Metrick MA, MacDonald G. 2016 Hofmeister ion-induced changes in water structure correlate with changes in solvation of an aggregated protein complex. *Langmuir* **32**, 1360–1369. (doi:10.1021/acs.langmuir.5b04489)
6. dos Santos AP, Levin Y. 2013 Surface and interfacial tensions of Hofmeister electrolytes. *Faraday. Discuss.* **160**, 75–87. (doi:10.1039/c2fd20067h)
7. Tobias DJ, Stern AC, Baer MD, Levin Y, Mundy CJ. 2013 Simulation and theory of ions at atmospherically relevant aqueous liquid-air interfaces. *Annu. Rev. Phys. Chem.* **64**, 339–359. (doi:10.1146/annurev-physchem-040412-110049)
8. Zuo Y, Chen H. 2003 Simultaneous determination of sulfite, sulfate, and hydroxyme- thanesulfonate in atmospheric waters by ion-pair HPLC technique. *Talanta* **59**, 875–881. (doi:10.1016/S0039-9140(02)00647-1)
9. Jungwirth P, Tobias DJ. 2006 Specific ion effects at the air/water interface. *Chem. Rev.* **106**, 1259–1281. (doi:10.1021/cr0403741)
10. Hey JC, Smeeton LC, Oakley MT, Johnston RL. 2016 Isomers and energy landscapes of perchlorate-water clusters and a comparison to pure water and sulfate-water clusters. *J. Phys. Chem. A* **120**, 4008–4015. (doi:10.1021/acs.jpca.6b01495)
11. Smeeton LC, Farrell JD, Oakley MT, Wales DJ, Johnston RL. 2015 Structures and energy landscapes of hydrated sulfate clusters. *J. Chem. Theory Comput.* **11**, 2377–2384. (doi:10.1021/acs.jctc.5b00151)
12. Smeeton LC, Hey JC, Johnston RL. 2017 Investigation of the structures and energy landscapes of thiocyanate-water clusters. *Inorganics* **5**, 20. (doi:10.3390/inorganics5020020)
13. Mylona S. 1996 Sulphur dioxide emissions in Europe 1880–1991 and their effect on sulphur concentrations and depositions. *Tellus B* **48**, 662–689. (doi:10.1034/j.1600-0889.1996. t01-2-00005.x)
14. Obrien JT, Prell JS, Bush MF, Williams ER. 2010 Sulfate ion patterns water at long distance. *J. Am. Chem. Soc.* **132**, 8248–8249. (doi:10.1021/ja1024113)
15. Brandt C, van Eldik R. 1995 Transition metal-catalyzed oxidation of sulfur(IV) oxides. Atmospheric-relevant processes and mechanisms. *Chem. Rev.* **95**, 119–190. (doi:10.1021/ cr00033a006)

16. Jou Sh, Shen My, Yu Ch, Lee Yp. 1996 Isomers of SO_3: infrared absorption of OSOO in solid argon. *J. Chem. Phys.* **104**, 5745–5753. (doi:10.1063/1.471335)

17. Eklund L, Hofer TS, Pribil AB, Rode BM, Persson I. 2012 On the structure and dynamics of the hydrated sulfite ion in aqueous solution—an ab initio QMCF MD simulation and large angle X-ray scattering study. *Dalton Trans.* **41**, 191–206. (doi:10.1039/c2dt12467j)

18. Cannon WR, Pettitt BM, Mccammont JA. 1994 Sulfate anion in water: model structural, thermodynamic, and dynamic properties. *J. Phys. Chem.* **98**, 6225–6230. (doi:10.1021/j100075a027)

19. Heinje G, Luck WP, Heinzinger K. 1987 Molecular dynamics simulation of aqueous $NaClO_4$ solution. *J. Phys. Chem.* **91**, 331–338. (doi:10.1021/j100286a020)

20. Wagner EL. 1962 Bond character in XYM-type molecules: chlorine–oxygen compounds. *J. Chem. Phys.* **37**, 751. (doi:10.1063/1.1733157)

21. Bader R 1994 *Atoms in molecules: a quantum theory*. Oxford, UK: Oxford University Press.

22. Valiev M *et al.* 2010 Nwchem: a comprehensive and scalable open-source solution for large scale molecular simulations. *Comput. Phys. Commun.* **181**, 1477–1400. (doi:10.1016/j.cpc.2010.04.018)

23. Jorgensen WL, Chandrasekhar J, Madura JD, Impey RW, Klein ML. 1983 Comparison of simple potential functions for simulating liquid water. *J. Chem. Phys.* **79**, 926. (doi:10.1063/1.445869)

24. Kazachenko S, Thakkar AJ. 2009 Improved minima-hopping. TIP4P water clusters, $(H_2O)_n$ with $n \leqslant 37$. *Chem. Phys. Lett.* **476**, 120–124. (doi:10.1016/j.cplett.2009.06.026)

25. Sanz E, Vega C, Abascal JLF, MacDowell LG. 2004 Tracing the phase diagram of the four-site water potential (TIP4P). *J. Chem. Phys.* **121**, 1165–1166. (doi:10.1063/1.1759617)

26. Wales DJ, Doye J. 1997 Global optimization by basin-hopping and the lowest energy structures of Lennard–Jones clusters containing up to 110 atoms. *J. Phys. Chem. A* **93**, 5111–5116. (doi:10.1021/jp970984n)

27. Rühle V, Stevenson J, Wales D. 2015 Python energy landscape explorer. See http://pele-python.github.io/pele/ (accessed 03/12/2015).

28. Trygubenko SA, Wales DJ. 2004 A doubly nudged elastic band method for finding transition states. *J. Chem. Phys.* **120**, 2082–2094. (doi:10.1063/1.1636455)

29. Takeuchi H. 2008 Development of an efficient geometry optimization method for water clusters. *J. Chem. Inf. Model.* **48**, 2226–2233. (doi:10.1021/ci800238w)

30. Shoemake K. 1985 Animating rotation with quaternion curves. *ACM Siggraph Comput. Grap.* **19**, 245–254.

31. Henkelman G, Jonsson H. 1999 A dimer method for finding saddle points on high dimensional potential surfaces using only first derivatives. *J. Chem. Phys.* **111**, 7010–7022. (doi:10.1063/1.480097)

32. Munro LJ, Wales DJ. 1999 Defect migration in crystalline silicon. *Phys. Rev. B* **59**, 3969–3980. (doi:10.1103/PhysRevB.59.3969)

33. Smeeton LC, Oakley MT, Johnston RL. 2014 Visualizing energy landscapes with metric disconnectivity graphs. *J. Comput. Chem.* **35**, 1481–1490. (doi:10.1002/jcc.23643)

34. Farrell JD, Wales DJ. 2014 Clusters of coarse-grained water molecules. *J. Phys. Chem. A* **118**, 7338–7348. (doi:10.1021/jp4119666)

35. Wang Lp, Head-Gordon T, Ponder JW, Ren P, Chodera JD, Eastman PK, Martinez TJ, Pande VS. 2013 Systematic improvement of a classical molecular model of water. *J. Phys. Chem. B* **117**, 9956–9972. (doi:10.1021/jp403802c)

36. Laury ML, Wang LP, Pande VS, Head-Gordon T, Ponder JW. 2015 Revised parameters for the AMOEBA polarizable atomic multipole water model. *J. Phys. Chem. B* **119**, 9423–9437. (doi:10.1021/jp510896n)